ELSEVIER

Shear Layer Vortices and Longitudinal Vortices in the Near Wake of a Circular Cylinder

J. Wu
Division of Building, Construction and Engineering, CSIRO, Highett, Australia

J. Sheridan
Department of Mechanical Engineering, Monash University, Clayton, Australia

K. Hourigan
Division of Building, Construction and Engineering, CSIRO, Highett, Australia

J. Soria
Department of Mechanical Engineering, Monash University, Clayton, Australia

■ Results are presented on (1) the shear layer vortices developing in the free shear layers located between the separation point and the first shed Strouhal vortex of a circular cylinder and (2) the longitudinal vortices developing in the braid region of the Strouhal vortices in the wake. Evidence based on flow visualization shows that the longitudinal vortices develop independently at low Reynolds numbers. An analysis is developed to show that the spanwise length scale of the longitudinal vortices in the separated shear layers and the longitudinal vortices in the Strouhal vortices are comparable near Re ≈ 1000. At higher Reynolds number, with increasing Re, the spanwise scale of the former reduces faster than that of the latter.

Keywords: *shear layer vortices, longitudinal vortices, spanwise length scale, wake*

INTRODUCTION

The shedding of Strouhal vortices from a circular cylinder results from the interaction of the two free shear layers separated from the cylinder. It is also known that small-scale vortices, because of the Kelvin–Helmholtz (KH) instability, develop in the separated free shear layers prior to the formation of Strouhal vortices. Bloor [1] appears to have been the first to observe these vortices (hereafter called shear layer vortices). She noted their similarity to the Tollmien–Schlichting waves observed in boundary layers and suggested their possible importance as a route in the transition to turbulence. Wei and Smith [2], using flow visualization and hot-wire anemometry, examined this phenomenon in the Reynolds number range 1200–11,000. They established a 0.87-power law relationship between the shear layer instability frequency and the Reynolds number. Kourta et al. [3], using hot-film anemometry and flow visualization, studied the problem in the Reynolds number range 2000–60,000. Shear layer instability waves were clearly identified in the power spectrum of velocity measured just downstream of the separation point.

Recent experimental observation has shown that spanwise vortices in plane free shear layers (mixing layers) develop three-dimensional vortices, generally referred to as longitudinal or streamwise vortices. Bernal and Roshko [4] showed that these longitudinal vortices are counterrotating vortices superimposed on the spanwise vortices in shear layers. This type of vortices will be called longitudinal vortices in shear layers.

Williamson [5] and Wu et al. [6], among others, showed another set of longitudinal vortices located in the Strouhal vortices. Wu et al. [6] showed that these vortical structures are counterrotating shear-aligned vortex structures superimposed on the vortex street in the braids joining consecutive Strouhal vortices. They will be referred to as longitudinal vortices in Strouhal vortices to differentiate them from the longitudinal vortices in shear layers.

Wei and Smith [2] proposed that the distortion of the shear layer vortices and subsequent stretching by the Strouhal vortices are responsible for the onset of the counterrotating longitudinal vortices. In doing so, they effectively conjectured that the shear layer vortices were the cause of the longitudinal vortices in the spanwise Strouhal vortices.

In the present paper, results are presented that characterize the shear layer vortices and the longitudinal vortices in Strouhal vortices. An analysis based on the present results and previous publications is developed that sheds new light on the relationship between the two vortex systems.

EXPERIMENTAL APPARATUS AND INSTRUMENTATION

Water Tunnel and Instrumentation

The majority of experiments were conducted in the return-circuit water tunnel at CSIRO in Australia. Water is pumped through a straight measurement section con-

Address correspondence to J. Wu, DBCE/CSIRO, P.O. Box 56, Highett, Vic 3190, Australia.

Experimental Thermal and Fluid Science 1996; 12:169–174

Published by Elsevier Science Inc. 1996
655 Avenue of the Americas, New York, NY 10010

0894-1777/96/$0.00
SSDI 0894-1777(95)00087-9

taining a calibrated orifice plate, through a diffuser, and into a settling chamber containing filter material and a honeycomb. The water then passes through a 4:1 contraction and a 660-mm-long straight square section before entering the working section. The working section is 770 mm long and 244 × 244 mm wide and has transparent walls made of acrylic. Water leaves the working section via a 440-mm-long duct from which it passes into an outlet reservoir tank. The free-stream velocity in the working section is uniform to within 1% outside the boundary layers at the walls. The spectrum of the fluctuating longitudinal velocity is free of sharp peaks and decreases in amplitude by 20 dB/Hz above 0.08 Hz, the longitudinal turbulence being typically 0.15%. Circular cylinders made of plexiglass, 244 mm long and with diameters of 6.4, 9.4, and 25.1 mm, were used for these measurements.

Local seeding of the flow with hydrogen bubbles was used for all flow visualization studies. The bubble stream was formed by electrolysis from an upstream-mounted nichrome wire (≈ 0.1 mm in diameter) cathode or from ribbon wires mounted flush with the surface of the models. To illuminate the flows, light from a 4-W (which was upgraded to 8 W in some of the later experiments) argon ion continuous-beam laser was spread into a light sheet using a cylindrical lens. Flow patterns were then recorded using a Videk digital CCD camera with a spatial resolution of 1280 × 1024 pixels. The digital image processing was undertaken with an Impro-II. Alternatively, still photographs were recorded on 35-mm films using a Nikon camera with a 55-mm lens.

Digital PIV Technique

A digital PIV method was used to measure the longitudinal vortices in a centerline plane $2D$ downstream from the cylinders. A review by Adrian [7] provides an excellent overview of the present status of PIV. The details of the method used here are available in a paper by Wu et al. [8], and only a brief description follows. Flow was seeded with white Q-CEL "hollow" microspheres with a mean diameter < 30 μm. The laser light was pulsed using a mechanical shutter. Light scattered from the particles in the laser sheet was recorded using the Videk digital CCD camera. The velocity field was extracted from the particle image on a Silicon Graphics workstation using an in-house digital PIV software system based on a digital Young's fringe method.

Wind Tunnel and Instrumentation

Some of the experiments were conducted in an open-jet wind tunnel. Air from a fan was directed through a diffuser into a settling chamber containing screens and a honeycomb. The air then passed through an 8:1 contraction to form an open jet with an outlet section 244 mm square. The operating range of the tunnel was 0–15 m/s. The mean velocity profile in the core of the jet was uniform to within ±0.5%, while the longitudinal turbulence level was typically 0.3% when bandpass-filtered between 0.1 and 2 kHz. An acrylic circular cylinder of 25.1-mm diameter and 244-mm length, fitted with two end plates, was used as a test model. A TSI hot-wire anemometer was used to measure time-mean velocity profiles across the shear layers separating from the cylinder and to detect velocity fluctuations in the near-wake region.

RESULTS

Shear Layer Vortices

The two free shear layers separating from a circular cylinder, with their velocity at the outer edge close to that of the free-stream flow and that at the inner edge practically zero, are observed to be unstable above a certain Reynolds number. Small-scale vortices due to the shear layer KH instability develop and merge into the Strouhal vortices. Typical vortex patterns of the separating shear layers of a circular cylinder using water tunnel flow visualization are shown in Fig. 1*a*. Figure 1*b* shows the conceptual ideal of the development of the shear layer vortices.

Figure 2 shows the longitudinal velocity fluctuation spectra at a number of x locations for a Reynolds number of 4400, obtained from the wind tunnel experiments. The origin of the x, y coordinate system coincides with the center of the cylinder. The Strouhal shedding frequency was 19.53 Hz at a free-stream velocity of $U_0 = 2.6$ m/s, which gives a nondimensional frequency of 0.19. A peak corresponding to the shear layer instability frequency at $f_{BG} \approx 133.0$ Hz can be found for $x/D > 0.7$ (the subscript BG is used in honor of Bloor and Gerrard, who were among the first to report the phenomenon). At Re = 4400 with $D = 25.1$ mm, the shear layer momentum thickness behind the separation point was $\theta \approx 0.35$ mm (calculated from the measured time-mean shear layer velocity profile), the frequency $f_{BG} \approx 133.0$ Hz, and the high-speed side velocity of the shear layer was found to be approximately

a

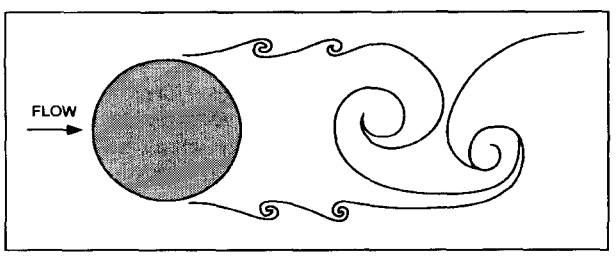

b

Figure 1. Flow visualization of the separating shear layer from a circular cylinder at $D = 25.1$ mm, Re = 2700. (*a*) Photograph; (*b*) conceptual diagram.

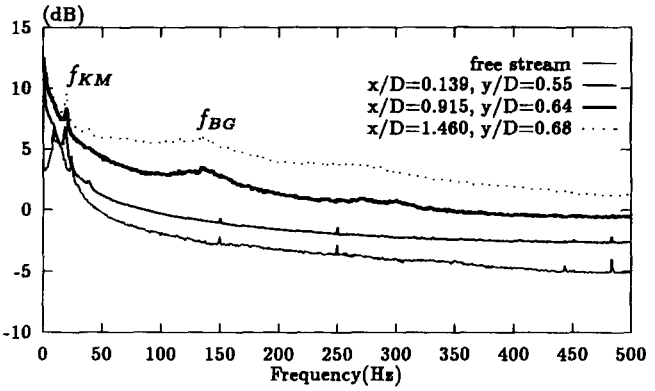

Figure 2. Velocity spectra of the separated shear layer of a cylinder; Re = 4400, D = 25.1 mm.

3.15 m/s, which gives a vortex convective velocity $U_c \approx$ 1.58 m/s. Using these results, a normalized shear layer vortex frequency can be estimated as $\theta f_{BG}/U_c \approx 0.030$. This is in reasonable agreement with linear stability theory [9], where the most amplified KH instability frequency for a plane mixing layer can be predicted using the equation

$$\theta f/U \approx 0.032, \quad (1)$$

where f is the instability frequency and U is the average velocity. The result indicates that the free shear layer separating from the cylinder exhibits the same instability mechanism as plane mixing layers.

Onset of Shear Layer Vortices

Tests were conducted in the water tunnel to establish the minimum Reynolds number for the onset of the shear layer vortices. The Reynolds number was gradually increased (and also decreased) to determine the existence of the shear layer vortices using flow visualization. It was determined that there is a transitional region, Re = 1000–3000, in which there is considerable uncertainty as to the existence of the shear layer vortices. Below this Reynolds number range, the shear layer vortices were not observable, while above it they were clearly observed. The precise value for the onset of the shear layer vortices is found to be dependent upon background disturbance; a high-turbulence background may cause a reduction in the critical Reynolds number.

It should be pointed out that Unal and Rockwell [10] found that a critical Reynolds number at which the shear layer vortices were seen to develop was Re ≈ 1900, whereas Bloor [1] found Re ≈ 1300. The discrepancy is quite large and could perhaps be attributed to a difference in the background disturbance conditions.

Longitudinal Vortex Structures

Another important class of vortices in the near-wake region comprises the longitudinal vortices developed in the braids joining consecutive Strouhal vortices [6]. Figure 3 shows mushroom-type structures along the cylinder axis in the near-wake region obtained using water tunnel flow visualization. The Reynolds number is 440, the diameter of the cylinder is 9.4 mm, and the cylinder is located on the left side of the picture. Flow is from left to right. The plane of view coincides with the plane containing the axis of the cylinder. The picture covers a spanwise area of approximately $12D$ (D is the cylinder diameter). The mushroom-type structures (indicated with the arrows) are indicative of the existence of counterrotating longitudinal vortices in the cylinder wake.

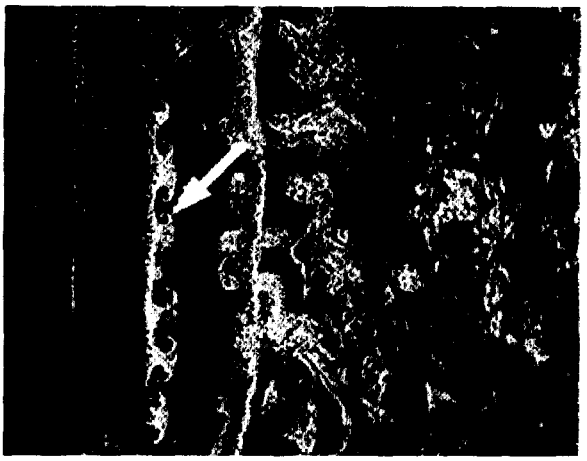

Figure 3. Longitudinal vortices in the wake of a circular cylinder, Re = 550.

To quantify the longitudinal vortical structures, multiple-exposure particle images were obtained at Re = 525 in the same plane but with much higher image magnification in order to resolve the fine-scale flow motions. The PIV image plane (Fig. 4*a*) covers a spanwise distance of $2.2D$ and is located $2D$ behind the cylinder. The instantaneous velocity field and sectional streamlines obtained from processing this particle image are shown in Figs. 4*b* and *c*. The cross-sectional streamline patterns were obtained by integrating the velocity field with a predictor-corrector scheme from a prescribed starting value. Bilinear interpolation of the measured velocity data was used in the integration. Features of the flow in this plane are several pairs of vortices spinning in opposite directions along the cylinder span. They are projections of inclined counterrotating longitudinal vortices being cut by the measurement plane.

The y component of vorticity (normal to the measurement plane) was found numerically from the instantaneous discrete velocity data. The probability density function (pdf) of the vorticity is calculated and plotted in Fig. 5, based on 50 frames of PIV images. The means of both positive and negative vorticity pdf distributions are approximately equal, $\xi_y \approx \pm 7.3$, where ξ_y is the vorticity normalized by U_0 and D and the subscript y denotes the y component. These data characterize the longitudinal vortices and the three-dimensionality of the vorticity field in cylinder wakes.

Onset of Longitudinal Vortices

The critical Reynolds number Re_{cr} for the onset of longitudinal vortices was investigated using flow visualization. Observations focused on the near-wake region extending up to $10D$ downstream of the cylinder. As the velocity was

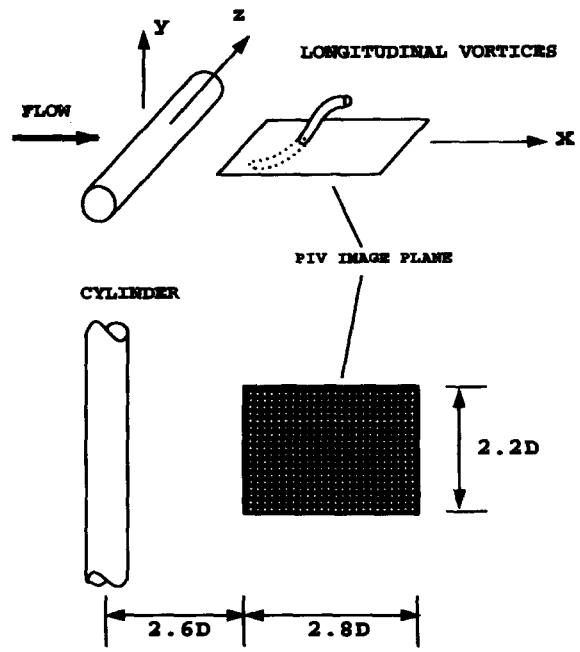

a

b

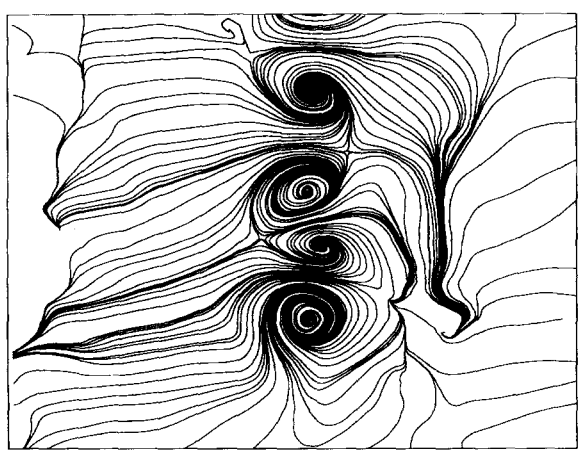

c

Figure 4. Longitudinal vortices in the wake of a circular cylinder, Re = 550. (*a*) PIV measurement plane; (*b*) velocity vector field; (*c*) sectional streamlines. Frame of reference: moving with the vortices at $60\%U_0$.

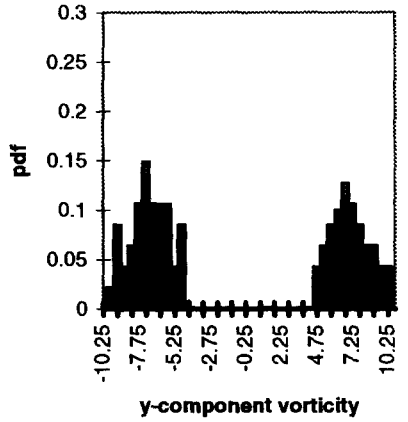

Figure 5. Probability density function of the maximum vorticity of longitudinal vortex pairs.

low for the Reynolds number range under investigation, it was possible to observe directly the onset of longitudinal vortices in the wake as the free-stream velocity was gradually increased. The tests were also conducted when the Reynolds number was reduced from above the critical Reynolds number until the longitudinal vortices disappeared completely. The tests were repeated several times during a week, and one month later, to establish repeatability and confidence in the results. Three different cylinder diameters (corresponding to three length-to-diameter aspect ratios of 74, 38, and 26), D = 3.3, 6.4, and 9.4 mm, were used during these tests.

The results are plotted in Fig. 6. The status of the longitudinal vortices is divided into three levels: nonexistent, intermittent, and existent, with digital representation of -1, 0, and $+1$, respectively. The intermittent status describes a situation where the vortices are found to exist intermittently. The longitudinal vortices were not observed below an intermittent region of Re $\approx$ 150–175 and were found to exist over the full cylinder span above this region.

It can be concluded that this range is significantly lower than the transitional Reynolds number range for the onset

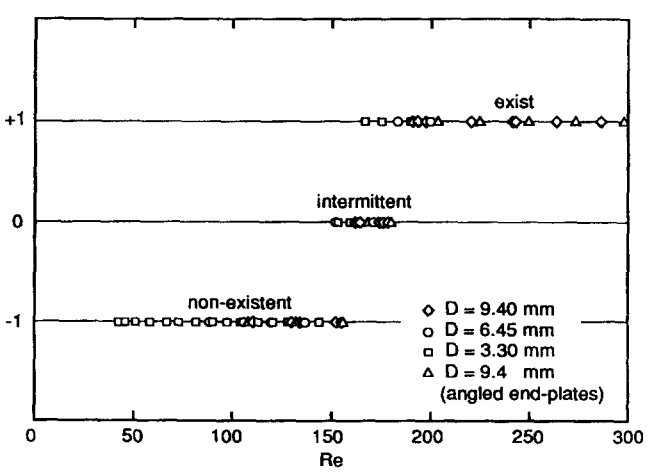

Figure 6. Onset of the longitudinal vortices: effect of Reynolds number. The existence of the longitudinal vortices: nonexistent, intermittent, and existent, represented by -1, 0, and $+1$, respectively.

of shear layer vortices discussed in the previous section. This led to an important conclusion: At low Reynolds numbers the longitudinal vortices in the Strouhal vortices develop independently, contrary to the suggestion of Wei and Smith [2].

In passing, it is interesting to note that Roshko [11], in his early comprehensive review of cylinder wakes, noted a transitional range of Re = 150–300 in which velocity measurements were erratic. It is proposed here that this transitional range is related to the longitudinal vortices discussed here and that Roshko's transition range is caused by the onset of the longitudinal vortices.

ANALYSIS OF SPANWISE LENGTH SCALE

When the Reynolds number is above 1000–3000, shear layer vortices will develop in the two free shear layers before merging into the Strouhal vortices. As has been previously observed, longitudinal vortices are known to be superimposed on the spanwise vortices that develop in plane mixing layers [4]. In the cylinder near wake, similar longitudinal vortices are expected to develop and to be superimposed on the shear layer vortices prior to the formation of the Strouhal vortices in the separated free shear layers for Re > 1000–3000.

To estimate the spanwise length scale of the longitudinal vortices in the separated free shear layers, the frequency of the shear layer vortices was measured by Sheridan et al. [12]. They reconfirmed the correlation suggested earlier by Kourta et al. [3]:

$$\frac{f_{BG}}{f_{KM}} = 0.095\ \mathrm{Re}^{0.5}, \tag{2}$$

where the subscript KM denotes the Karman vortices, and $f_{KM} \approx 0.2U_0/D$. The convective velocity of the shear layer vortices was assumed to be $U_c = (U_1 + U_2)/2$, where U_1 and U_2 are flow velocities on the high- and low-speed sides of the shear layer. Assuming that $U_2 \approx 0.0$ and $U_1 \approx 1.3U_0$, $U_c \approx 0.65U_0$. The streamwise wavelength of the shear layer vortices can be estimated to be

$$\lambda_{BG} = \frac{U_c}{f_{BG}} = \frac{0.65U_0}{0.095\,\mathrm{Re}^{0.5} f_{KM}} = \frac{34D}{\mathrm{Re}^{0.5}}, \tag{3}$$

or

$$\frac{\lambda_{BG}}{D} = \frac{34}{\mathrm{Re}^{0.5}}. \tag{4}$$

In contrast, we note that the longitudinal vortices that develop on top of the spanwise vortices in a mixing layer have a wavelength ratio (ratio of spanwise wavelength of the longitudinal vortices to streamwise wavelength of the primary vortices upon which the former develop) of 0.67 [4]. Assuming the same wavelength ratio between these two types of vortices in the separating shear layer results in

$$\lambda_{BG3} = 0.67\lambda_{BG}, \tag{5}$$

where λ_{BG3} is the spanwise wavelength of the three-dimensional vortices superimposed on the shear layer vortices (i.e., longitudinal vortices in shear layers). Substituting the expression for λ_{BG} into Eq. (5) gives

$$\frac{\lambda_{BG3}}{D} = \frac{23}{\mathrm{Re}^{0.5}}. \tag{6}$$

The spanwise wavelength of longitudinal vortices in the Strouhal vortices were also measured using the water tunnel facility in the Reynolds number range 250–1800. The distances between pairs of mushroom-type structures recorded on digital images were measured directly using the image-processing software. The two spanwise wavelength curves, representing those of longitudinal vortices in the separated free shear layers and those in the Strouhal vortices, are graphed in Fig. 7.

It is seen that for Re > 2000 the two structures have quite different spanwise length scales, suggesting that they might be effectively decoupled. As the Reynolds number is increased, the spanwise length scale of the longitudinal vortices in shear layers reduces faster than those in the Strouhal vortices. However, when the Reynolds number is reduced to Re ≈ 1000, the two curves intersect, indicating that the two structures have comparable spanwise length scales. It is noted that below Re = 1000 the shear layer vortices are usually suppressed and the curves only represent the case when external forcing was used to excite the shear layer vortices.

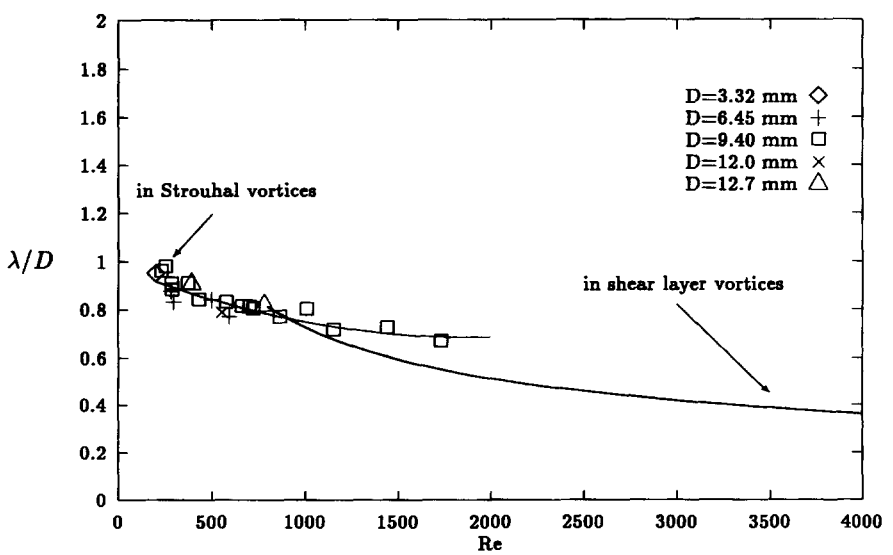

Figure 7. A comparison of spanwise wavelength: streamwise vortices in the separated shear layers and in the Strouhal vortices, where λ is the spanwise wavelength normalized by the cylinder diameter D and Re is the Reynolds number.

DISCUSSION

The development of small-scale free shear layer vortices and of counterrotating longitudinal vortices in the braids joining consecutive Strouhal vortices are the main features of near-wake vortex dynamics. The results presented in this paper show that the onset of the two types of vortices is Reynolds number–dependent and that the critical Reynolds numbers for these two types of vortices to appear are significantly different. The results indicate that longitudinal vortices develop independently from the shear layer vortices at low Reynolds numbers, as the former have a much lower critical Reynolds number than the latter. This result is contrary to the assertion of Wei and Smith [2] that the shear layer vortices are the cause of the longitudinal vortices embedded in the Strouhal vortices.

Through a simple analysis, the spanwise length scale of the two types of longitudinal vortices are presented. It is interesting to note that in the higher Reynolds number range, Re > 2000, the spanwise length of these two types of longitudinal vortices is significantly different. The difference becomes more pronounced as Re is increased; the spanwise length scale of the longitudinal vortices in shear layers reduces faster than that of the longitudinal vortices embedded in the Strouhal vortices. The matching of the wavelength only occurs near Re $\approx$ 1000.

PRACTICAL SIGNIFICANCE

A better understanding of the mechanism of the vortical structures in the wake of a bluff body is critical for improved design and operation of numerous industrial devices, such as heat exchangers, offshore structures, and mixing equipment, where wakes and shear flows play a major role. The present paper provides information and analyses of a number of types of vortices developing in the near-wake region. The results assist in the better understanding of near-wake vortex dynamics.

CONCLUSION

In conclusion, some experimental results and analyses have been presented in an attempt to characterize the shear layer vortices and the longitudinal vortices located in braids joining consecutive Strouhal vortices. It is shown that the critical Reynolds numbers of the two types of vortices are significantly different and that the latter develops independently of the former at lower Reynolds number (e.g., Re = 170). At higher Reynolds numbers, the spanwise length scale of the two types of longitudinal vortices, those superimposed on the separated free shear layer vortices and those superimposed on the Strouhal vortices, is significantly different.

Support from an Australia Research Council grant is gratefully acknowledged. J. Wu wishes to acknowledge the support from a Monash University scholarship.

NOMENCLATURE

D	cylinder diameter, mm
f_{BG}	frequency of shear layer vortices, Hz
f_{KM}	frequency of Karman vortices, Hz
Re	Reynolds number based on free-stream velocity and cylinder diameter, dimensionless
U_0	free-stream velocity, m/s

Greek Symbols

λ	spanwise wavelength of the streamwise vortices, superimposed on Karman vortices, mm
λ_{BG}	streamwise wavelength of the shear layer vortices, mm
λ_{BG3}	spanwise wavelength of the streamwise vortices, superimposed on shear layer vortices, mm
θ	shear layer momentum thickness, mm

REFERENCES

1. Bloor, M. S., The Transition to Turbulence in the Wake of a Circular Cylinder, *J. Fluid Mech.* **19,** 290–304, 1964.
2. Wei, T., and Smith, C. R., Secondary Vortices in the Wake of Circular Cylinders, *J. Fluid Mech.* **169,** 513–533, 1986.
3. Kourta, A., Boisson, H. C., Chassaing, P., and Minh, H. H., Nonlinear Interaction and the Transition to Turbulence in the Wake of a Circular Cylinder, *J. Fluid Mech.* **181,** 141–161, 1987.
4. Bernal, L. P., and Roshko, A., Streamwise Vortex Structure in Plane Mixing Layers, *J. Fluid Mech.* **170,** 499–525, 1986.
5. Williamson, C. H. K., The Existence of Two Stages in the Transition to Three-Dimensionality of a Cylinder Wake, *Phys. Fluids* **31**(11), 3165–3168, 1988.
6. Wu, J., Sheridan, J., Soria, J., and Welsh, M. C., An Experimental Investigation of Streamwise Vortices in the Wake of a Bluff Body, *J. Fluids Struct.* **8,** 621–635, 1994.
7. Adrian, R. J., Particle-Imaging Techniques for Experimental Fluid Mechanics, *Annu. Rev. Fluid Mech.* **23,** 261–304, 1991.
8. Wu, J., Sheridan, J., Soria, J., and Welsh, M. C., An Investigation of Unsteady Flow Behind a Circular Cylinder Using a Digital PIV Method, in *Laser Anemometry, Advances and Applications,* ASME FED-Vol. 184, pp. 167–172, 1994b.
9. Ho, C. M., and Huerre, P., Perturbed Free Shear Layers, *Annu. Rev. Fluid Mech.* **16,** 365–424, 1984.
10. Unal, M. F., and Rockwell, D., On Vortex Formation from a Cylinder. Part 1. The Initial Instability, *J. Fluid Mech.* **190,** 491–512, 1988.
11. Roshko, A., On the Development of Turbulent Wakes from Vortex Streets, NACA Rep. 1191, pp. 801–825, 1955.
12. Sheridan, J., Soria, J., Wu, J., and Welsh, M. C., The Kelvin–Helmholtz Instability of the Separated Shear Layer from a Circular Cylinder, in *Bluff-Body Wakes, Dynamics and Instabilities,* IUTAM Symp., pp. 115–118, 1992.

Accepted August 24, 1995